Chapter 5

Combination of Lithography and Coating Methods for Surface Wetting Control

Athanasios Milionis, Ilker S. Bayer, Despina Fragouli, Fernando Brandi and Athanassia Athanassiou

Additional information is available at the end of the chapter

http://dx.doi.org/10.5772/56173

1. Introduction

In recent years, many different lithographic approaches have been applied in order to fabricate micro and nano-structures which are successfully used for the formation of surfaces with special wetting properties [1,2]. In fact, the modification of the surface roughness in the micron, sub-micron and nano-scale with or without chemical treatment, results in surfaces with controlled wetting properties exhibiting the extreme limits (e.g. superhydrophobic, superhydrophilic surfaces) [3-5]. In this work, we examine different approaches in order to achieve such patterned surfaces with tunable wetting characteristics. In particular, we fabricate micro-rough substrates by using different lithographic techniques. As an additional step, these substrates are coated with different types of sub-micrometer particles or nanoparticles (NPs) (organic or inorganic) in order to achieve the desired chemical modification and to induce submicron or nano-roughness to the surfaces. Specifically, the coatings consist of polytetrafluoroethylene (PTFE) sub-micrometer particles and iron oxide colloidal NPs and they are applied by using triboelectric (fricition induced) or spray deposition. Apart from their interesting wetting properties from the theoretical point of view, such type of surfaces can be used in various applications such as in biological scaffolds, microfluidics, lab-on-a-chip devices and aerospace vehicles [6-9].

The first part of this study refers to the use of the appropriate lithographic technique so as to obtain a controlled rough surface on soft polymeric or hard substrates. Common lithographic techniques that have been used successfully for this purpose are UV lithography, laser-micromachining, electron-beam lithography, soft-lithography, X-ray lithography, plasma etching etc [10-17]. The main advantage of the lithographic techniques is the creation of well-defined patterned structures with controllable geometrical characteristics.

The second step is to induce additional sub-micron or nano-roughness and to chemically modify the patterned surfaces by adding layers of organic or inorganic particles. This provides an important aspect for tailoring the wetting characteristics of the surface since the chemistry is being modified together with the topography. In order to do this a thin coating layer can be deposited on top of the surface by different coating methods such as drop casting, chemical vapor deposition, spray coating, triboelectric deposition, etc.

Herein, we present two different methods for constructing surfaces with tunable wetting properties, both of them based on the concept of combining a lithographic technique to create an initial micro-rough surface and a deposition technique in order to add sub-micron or nano-rough features using particles with different chemical properties. In particular, the approaches are:

1. UV lithography with spray coating: At first, a pattern of equally sized square micro-pillars is fabricated by photopolymerizing an SU-8 photoresist and as a second step different types of particles are sprayed on top by using a spray coating setup. The particles are PTFE sub-micrometer particles and iron oxide NPs that are sprayed in successive coating layers. The different size and chemistry of the particles are responsible for the tuning of the wetting characteristics of the substrates.
2. Laser micromachining with triboelectric deposition: Silicon surfaces are micro-textured by laser ablation with a nanosecond pulsed UV laser and subsequently triboelectrically charged PTFE particles are deposited on them. Again the wetting properties are examined and they are compared with the micro-textured silicon carbide (SiC) surfaces which have been processed in a similar manner.

The morphology of the surfaces is characterized by means of atomic force microscopy (AFM) and scanning electron microscopy (SEM). In order to characterize the wetting properties, the apparent water contact angles (APCA) and the water contact angle hysteresis (CAH) are measured. The fabrication processes of the patterns are relatively quick and simple, making them good candidates for commercial production. Possible uses of such kind of materials can expand from self-cleaning surfaces, microfluidic devices and smart surfaces to biotechnological applications.

2. Combination of UV lithography and spray coating

Lithographic patterning using UV light is a very attractive technology due to the relatively low energy consumption, room temperature operation, rapid curing, spatial control and the ability to expose in a single step large surface areas [18]. For these reasons UV lithography is nowadays the most widespread used method for microfabrication.

The UV lithography technique involves various steps and it is suitable for processing materials that are called photoresists and absorb in the UV region of light. The common fabrication steps can be summarized as resist coating, pre-bake, mask alignment, exposure and development. Initially the substrate has to be cleaned with different chemicals to avoid the presence of dust,

http://dx.doi.org/10.5772/56173

lint, bacteria, water and oil. Then the photoresist is applied by spin-coating, forming a uniform layer on the substrate. Its thickness depends on the speed of the spinning. Subsequently, the photoresist is baked on a hot plate or in a convection oven in order to evaporate its solvent. After this, the sample is aligned with the UV light source by using a mask aligner and it is exposed through a photomask that contains the design of the pattern to be transferred. The role of the photomask is to allow the UV light to pass only from some specific regions and to block it from others. When the sample is exposed, the development stage takes place. In this stage, chemicals are applied to the surface causing a positive or a negative photoresist reaction. In the case of the negative reaction the molecules that were subjected to UV light are bonded strongly, causing the polymerization of the material. The use of appropriate chemicals will remove the non-polymerized sections. In the positive reaction, the sections of the photoresist that were exposed are chemically altered and decomposed and after chemically washing them, the non-exposed parts remain on the substrate. In some occasions, in the development stage, a post exposure bake is required before the use of the chemicals in order to complete the chemical reaction that started during the exposure of the photoresist.

Spray coating is a standard method to apply thin coatings on surfaces. A spray coating setup consists of a high-pressure airstream flow that is able to break a liquid into miniature aerosol droplets through a confined nozzle head. The liquid is the coating to be deposited on the substrate and it is stored on a glass vial that is connected with the nozzle head. The main advantage of the spray coating compared to other coating techniques, is that the sprayed solution dries immediately after its deposition on the target, preventing thus possible aggregations and coating inhomogeneities that can occur during the evaporation of the solvent as in other methods (e.g. drop casting). In this way, the sprayed coatings are uniform while the preparation time is reduced.

The combination of the UV photolithography with the spray coating technique can be a very efficient way to create surfaces with hierarchical roughness in the micro, sub-micron and nanoscale that are necessary in order to obtain surfaces with tunable wetting characteristics [4,19]. Both techniques are fast and simple and are successfully used in the industry in the last decades.

2.1. Fabrication procedure and materials used

The material used as a polymeric substrate for the UV lithography, is the SU-8 3050 from Microchem, USA. SU-8 is a commercial biocompatible epoxy-based photoresist that is suitable for the microfabrication of high aspect-ratio hierarchical structures with smooth and vertical sidewalls, and it is used widely in the fabrication of MEMS devices, waveguides, microfluidic devices and stamps. It absorbs in the UV range of the spectrum with a maximum efficiency at 365 nm. When exposed to UV light, its molecular chains crosslink causing the polymerization of the material that becomes strong, stiff and chemically resistant. SU-8 has been also used for the fabrication of dual-scale rough structures. Such hierarchical structures produced with SU-8 have been coated with titanium dioxide, PTFE submicrometer particles and fluorocarbons in order to obtain surfaces with special wetting properties [19-21].

To fabricate the SU-8 patterns initially we dispensed a small quantity of the SU-8 3050 onto a silicon wafer. Then the spin-coating of the SU-8 was accomplished in two subsequent steps: (a) at 500 rpm for 10 s with spinning acceleration of 100 rpm/s and (b) at 4.000 rpm for 30 s with spinning acceleration of 300 rpm/s. The samples were pre-baked at 100 °C for 20 min on a hotplate. The thickness of the film obtained was 33 μm. A sodalime mask of square-shaped patterns (42 μm side) from Deltamask, Netherlands, with inter-square distance of 28 μm, was used for the exposure of the spin-coated samples. Patterning was performed by exposing the spin-coated material to UV radiation with a Karl-Suss MA6 mask aligner in hard contact mode with an i-line mercury lamp. An exposure dose of 323 mJ was used to fully polymerize the 33-μm-thick SU-8 layer. The exposure was followed by a post-exposure bake on a hotplate at 65 °C for 1 min and at 95 °C for 5 min, in order to achieve complete cross-linking of the resist. The samples were then allowed to cool down in order to improve the adhesion of SU-8 to the silicon wafer. Subsequently, the samples were washed for a couple of minutes with SU-8 developer followed by rinsing with 2-propanol. Following this process square SU-8 pillar structures of 33 μm height and 28 μm inter-pillar distance were obtained. In Figure 1 there is a schematic representation with the steps followed for the fabrication of the patterned surfaces.

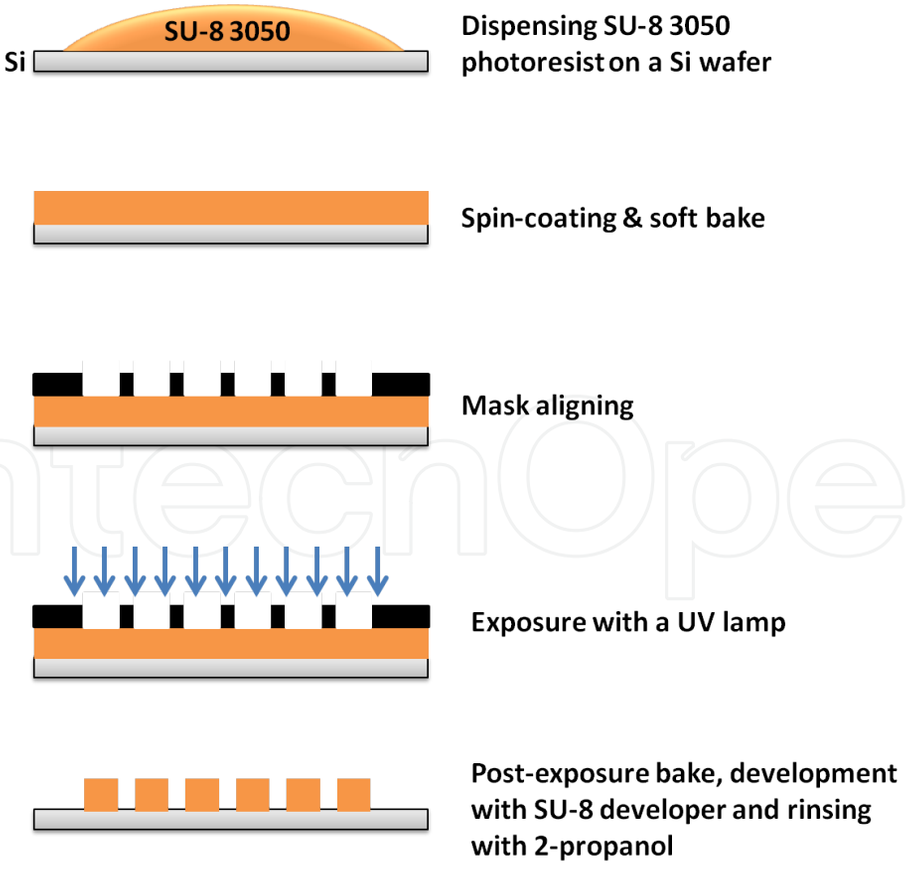

Figure 1. Schematic illustrating the various steps followed for the fabrication of the SU-8 micropillars.

http://dx.doi.org/10.5772/56173

In order to modify the surface chemistry and to induce different scales of roughness to the hierarchical SU-8 micro-patterns, the spray-coating technique was used. In particular, colloidal solutions of PTFE sub-micrometer particles and iron oxide NPs are used to form a first and a second coating layer respectively. Like this, sub-micron and nano- roughness is added on top of the SU-8 micro-patterns.

Regarding the preparation of the colloidal solutions, the PTFE powder, purchased from Sigma-Aldrich with an average particle diameter of ~ 150 nm, was dispersed in acetone (3% wt.) and sonicated for about 20 minutes in order to form a uniform and well-dispersed suspension. The nearly spherical colloidal iron oxide NPs (average diameter: 24±3 nm) are dispersed in chloroform (0.06% wt.) and they are synthesized in our lab [4]. The colloidal solutions were sprayed, as shown in Figure 2, at a distance of 10 cm from the substrate while the pressure of the airstream was 150 kPa. The resulting surface, after all this treatment, exhibits a triple-scale roughness in micro-, submicron- and nano-scale. Moreover, the specific treatment induces significant changes in the surface chemistry, since the PTFE particles are well-known for their hydrophobic properties. The iron oxide NPs are also hydrophobic due to the oleic acid (OLAC) molecules that are used as surfactants [22]. Thus, the sprayed particles have a dual role in the system, which is to increase the hydrophobicity and also to change the roughness scale of the patterns.

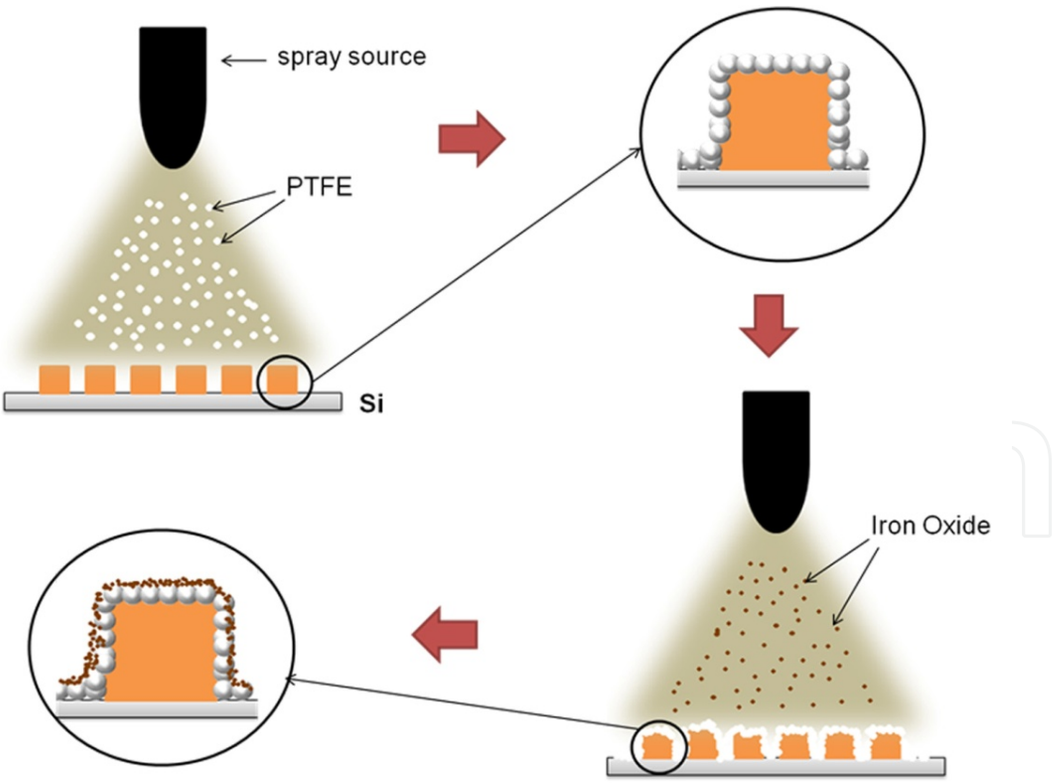

Figure 2. Schematic illustrating the successive coating steps. At first the PTFE solution is sprayed on the substrate with the SU-8 micropillars (top panel). As a second step, the iron oxide NPs are sprayed on top of the SU-8/PTFE micro/submicron rough pattern, thus inducing a three-scale roughness [4].

2.2. Characterization and discussion on the morphology and wetting behavior

In order to characterize the wetting properties of the samples, APCA and tilting angle measurements were taken using a KSVCAM200 contact angle goniometer, Kruss, Germany. The area of the water drop (total drop volume: 10 μl) in contact with the surface was sufficient enough to experience the periodicity of the pattern. The tilting angle measurements were performed by recording the images of the droplets while the underlying substrates were inclined by a tilting base. All measurements were taken a few seconds after the placement of the water droplets.

Scanning electron micrographs were collected with a Nova NanoSEM200 scanning electron microscope (SEM) by FEI Instruments. Low-vacuum configuration was used with a chamber pressure of 0.3 mbar. To decrease the charging effects on the surface of the samples, a flux of water vapor was injected in the chamber. In Figure 3 we present the SEM images of the SU-8 micro-pillars with the different coatings, in high and low resolution, together with the corresponding APCAs.

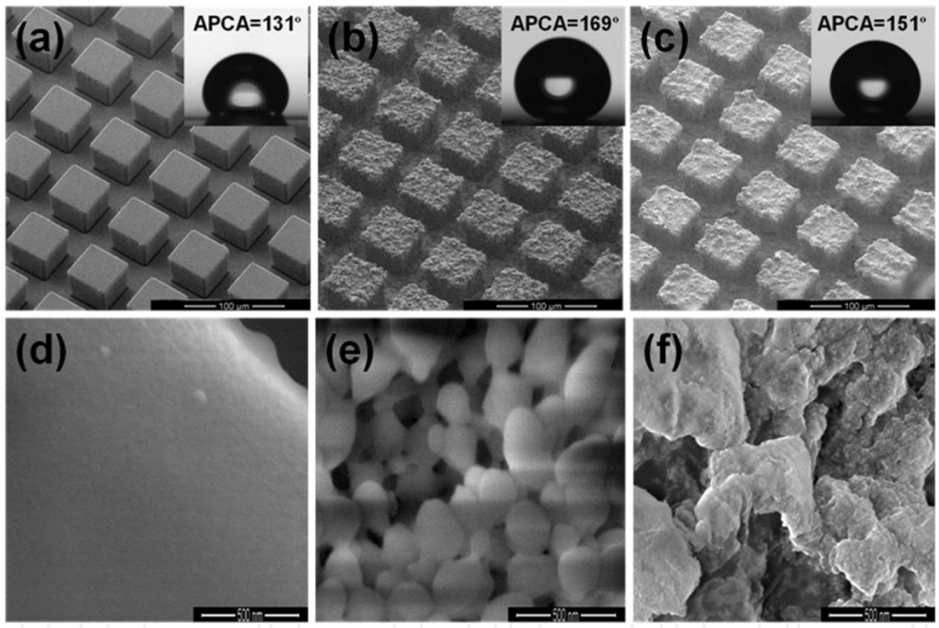

Figure 3. Low-magnification tilted-view SEM images of (a) SU-8 micro-pillars, (b) SU-8 micro-pillars with PTFE sub-micrometer particles sprayed, (c) SU-8 micro-pillars with iron oxide NPs sprayed as a second layer, on top of the already sprayed PTFE sub-micrometer particles. Insets: the APCA of the surface in each case. In (d), (e) and (f) they are presented high-magnification top-view images of the surface of each micro-pillar corresponding to (a), (b) and (c) respectively [4].

As shown in Figure 3, the initial SU-8 uncoated pattern displays an APCA of 131°±7° (Figure 3a and d), significantly higher compared to the APCA measured on the corresponding flat SU-8 surface, (82°±2°). Moreover, this pattern is highly adhesive to water since the droplets stay on the substrate even for 180° tilt. When the PTFE sub-micrometer particles are sprayed on the pillars, the morphology of their surface changes dramatically (Figure 3b and e). In fact, the pillars retain their micro-scale geometrical characteristics, but on top they exhibit sub-

http://dx.doi.org/10.5772/56173

micrometer roughness due to the presence of the PTFE particles. The combination of the micro/submicron roughness with the well-known water-repellent properties of the PTFE makes the patterned surfaces superhydrophobic and self-cleaning with an APCA of 169°±2° and sliding angle ≤1°. In fact, in the absence of the micro-roughness, e.g. at the flat SU-8 surface coated with PTFE particles, the APCA is lower (159°±8°) while the sliding angle ≤ 10°, demonstrating the importance of the micro-patterning.

By using the PTFE-sprayed micro-pillars as a substrate for the successive spraying of a coating of iron oxide NPs, surfaces with micro-, submicron- and nano-roughness can be obtained (SEM images of Figure 3c and f). The underlying PTFE particles seem to be fully covered by the iron oxide NPs. The latter do not appear well separated but rather as a homogeneous coating. After this coating the APCA remains superhydrophobic (151°±6°) (APCA of the flat surface 140° ±10°) but on the other hand the water adhesion is dramatically increased. Indeed the substrates become "sticky" even for 180° substrate tilt angles (Figure 4). Such type of surfaces, that have a very high APCA while at the same time exhibit very high adhesion to water, can be designated as "sticky superhydrophobic" surfaces [23,24]. This state has been also reported as "petal effect" in some part of the literature [25,26].

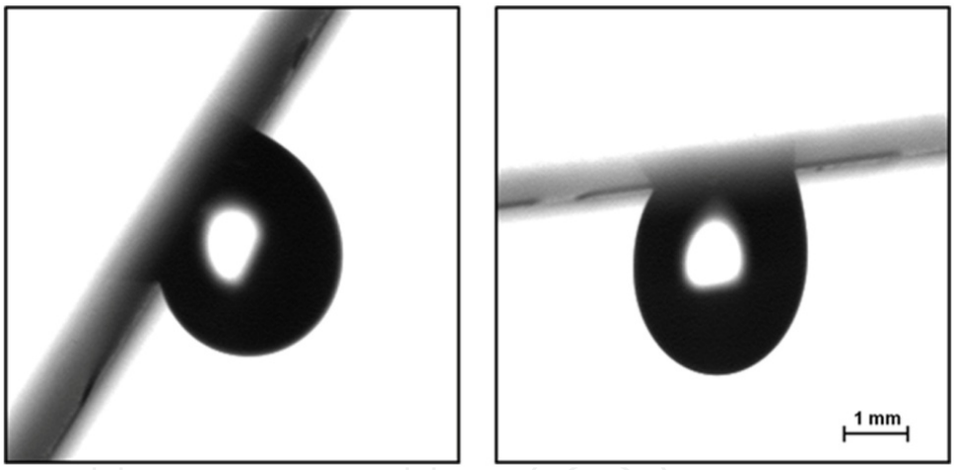

Figure 4. Water drops that remain adhered in an iron oxide/PTFE/SU-8 patterned surface under very high substrate inclinations (tilt angle: 122° on the left image and 173° on the right) [4].

To explain the abovementioned results we will compare them with the well-known Cassie-Baxters' theoretical model [27]. The Cassie-Baxter model is generally applied to predict the APCA on a rough hydrophobic surface and it particularly assumes that a water droplet can wet a surface only partially, due to the trapping of air pockets underneath the droplet at the recessed regions of the surfaces. For such hierarchical surfaces, like the ones fabricated, the water contact angle (WCA) predicted from the Cassie-Baxters' model can be extracted by the following equations [28]:

$$\cos\left(\theta_{CB}\right) = f_s\left[\cos\left(\theta_Y\right) + 1\right] - 1 \quad (1)$$

$$f_s = \frac{1}{\left(\frac{b}{a} + 1\right)^2} \quad (2)$$

where f_s is the fraction of the solid surface in contact with the droplet and θ_Y is the Young's angle, i.e., the contact angle of the droplet on the corresponding flat surface with the same chemical characteristics. a is the width of the pillars (a=42 μm) and b is the spacing (b=28 μm) between the pillars. The predicted WCA values from Equation (1) for the surface of the coated and uncoated SU-8 micropillars are presented in the Table 1.

Material	APCA/° (flat surface)	APCA/° (patterned surface)	Cassie-Baxter/°
SU-8	82±2	131±7	126
SU-8+PTFE	159±8	169±2	167
SU-8+PTFE+Iron oxide	140±10	151±5	156

Table 1. APCA values of the flat and patterned surfaces and their extracted theoretical values from the Cassie-Baxter model for the three surfaces. The theoretical values were extracted from the flat SU-8 surfaces coated with the same particles as the patterned ones [4].

As shown in Table 1, the Cassie-Baxter model predictions match with the values obtained experimentally. This means that the droplets rest on a surface containing air pockets. However, in terms of water adhesion, the highly sticky uncoated patterns are converted to non adhesive after the application of the PTFE coating. After the subsequent iron oxide coating the superhydrophobic patterns become again highly adhesive. Since the experimental values of all the three cases are in accordance with the Cassie-Baxter model, we must exclude the possibility that there is a complete wetting state (Wenzel) that would increase the water adhesion due to the pinning effects arising from the penetration of the droplet in the inter-pillar spacing. Instead, the capillary effects seem to occur in the upper part of the pillars and are provoked by the final nano-rough coating layer of iron oxide, while the inter-pillar spacing continues to be filled with air. In fact, similar studies that describe such a pinning state occurring in nano-rough hierarchical surfaces have already been published [29-31]. These works present composite micro- and nano-rough systems where the pinning effects take place only in the nano-rough surface while in the micro-scale the wetting state obeys the Cassie-Baxter model.

In summary, after the coating of iron oxide NPs it is possible to fabricate triple-scale rough superhydrophobic surfaces with high water adhesion, and on the other hand it is possible to obtain dual-scale rough SU-8/PTFE coated superhydrophobic surfaces with ultralow adhesion. If an additional layer of PTFE particles is applied on top of the iron oxide coating, the low adhesion state can be recovered again. In such a manner, with successive spray coatings, of PTFE and iron oxide particles, one can obtain surfaces with alternating water adhesion properties on superhydrophobic layers.

http://dx.doi.org/10.5772/56173

3. Laser micromachining and triboelectric deposition

Laser micromachining is a term that includes a variety of processes including hole drilling, ablation, milling, and cutting of soft or hard materials using laser light sources. Specifically laser ablation, is a technique where a focused pulsed laser beam is used in order to remove material from a solid target [32] and thus to modify the morphological features of its surface. In fact, the high energy flux of the pulsed laser beam focused on the target results in the photon absorption by the electrons of the system and in the electrostatic instability of the lattice ions. As a consequence the ejection of the interacting material is induced in the form of plasma and hence the ablation leaves a void in the laser focus region. This lithographic technique is nowadays used widely in the industry for the fabrication of MEMS/NEMS, CMOS, 3D-microstructures, micro-trenches, micro-channels, micro-holes, sub-micrometer gratings, nanophotonics and surfaces dedicated to bacterial activity [33,34]. Laser ablation, apart from the microstructuring of surfaces, has also been used alternatively as a technique to produce NPs by irradiating solid targets [35]. Its main advantages when compared with other lithography techniques are the fast material processing speed, large scan area and single-step capability. Compared to the previous lithography technique described before (UV lithography), this one requires less processing steps and also the use of chemicals is much more limited. However it cannot form ordered and well controlled micron sized features. Nevertheless the laser ablation technique is able to induce roughness on a surface, and subsequently modify its wetting characteristics.

Triboelectric particle deposition is a coating technique based on the physical phenomenon of frictional (or contact) charging of dissimilar materials [36,37]. In other words, during contact, certain materials become electrically charged when they come in contact with another material through friction. It is possible to deposit small polymer particles on a surface by sandwiching them between two surfaces and rub them against one another. In this way, a uniform coating can be obtained on one of the surfaces due to the self-assembly of the particles that they are attracted with electrical forces. The main advantage of this coating method is that it is a dry technique, based on physical concepts and does not require the use of hazardous chemicals.

The laser micromachining can be combined with the triboelectric deposition in order to fabricate surfaces with different roughness scales and different wetting properties [5]. The roughness parameters of the fabricated surfaces can be controlled by tuning the laser parameters such as laser power and focal length, and also by changing the amount of particles deposited during the coating. Both of these techniques are efficient and rapid, and for these reasons their combination can be a potential industrial method for fabricating coatings with special wetting properties.

3.1. Fabrication process and materials

The substrates used in this study are commercial standard silicon wafers (one side polished) having natural oxide surface layers. Both polished and unpolished sides of the wafers were used for laser micromachining. In particular a UV nanosecond laser beam was focused using a cylindrical lens with a focal length of 75 mm. The laser fluencies tested were ranging from

0.5 up to 2 J/cm^2. During the ablation process the silicon wafers were stored in liquid bath of methanol or distilled water with 5 mm of liquid covering their surface. The wafers were moved in precise small steps with an x-y translation stage until a textured surface region of approximately 1 cm^2 was obtained. In Figure 5 there is a schematic representation of the laser micromachining setup. After the ablation, the wafers were removed from the liquid baths and left to dry under ambient conditions.

Apart from the textured silicon wafers, as substrates, we also used various micro-textured silicon SiC surfaces. Typical sandpapers of 600, 800 and 1200 grit sized were used.

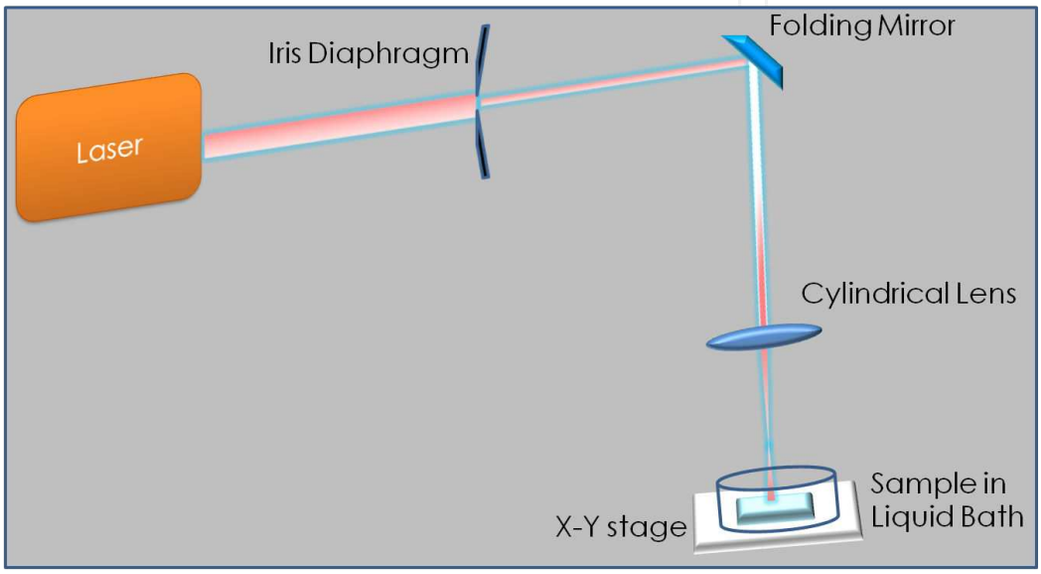

Figure 5. Schematic representation of the laser micromachining setup.

For the coating of the textured silicon wafers, as discussed in Chapter 2, sub-micrometer PTFE particles were used. Certain amount of PTFE powder was spread over commercial Scotch Brite (3M) medium duty cellulosic foam with dimensions 15 cm × 9 cm × 2 cm. A metal rod was used to rub the PTFE powder on the foam surface for a few minutes, in order to spread it uniformly. Subsequently, the foam was continuously rubbed against the textured silicon surfaces in circular motion for a few minutes. At the end of this process, almost all the PTFE particles were transferred to the textured silicon surface forming a thin PTFE layer. It was found that the PTFE particles were strongly attached onto the laser-formed structures, since the post treatment (immersion in different solvents such as acetone, toluene, methanol or chloroform) did not cause particle removal from the surfaces. Figure 6 shows a sketch illustrating the basic steps followed for the triboelectric deposition of the PTFE particles.

A slightly different coating approach was used to apply the PTFE coating on the SiC sandpapers. The PTFE powder was directly deposited on the sandpapers and a cellulosic foam was rubbed over the surfaces directly, for a few minutes, to spread the PTFE particles over the rough surface.

http://dx.doi.org/10.5772/56173

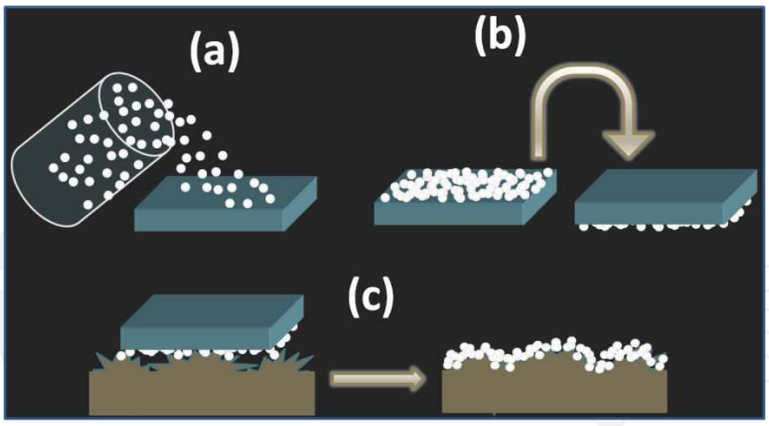

Figure 6. Schematic illustrating the triboelectric deposition of the PTFE particles on textured silicon. (a) The PTFE powder is spread over the foam. (b) The PTFE powder is distributed uniformly with the use of a metal rod. (c) The PTFE particles are rubbed against the textured silicon surface and finally they are transferred to the silicon forming a thin layer.

3.2. Characterization, results and discussion

The morphology of the laser-textured surfaces was inspected with SEM. Figure 7 shows the SEM images of the laser patterned surfaces obtained on the polished surface of a silicon wafer. Densely packed pyramid-like roughness features (pillars with density of 0,8 pillar/μm) of the order of 2 μm in size were produced on the surface.

The topography of the textured surfaces was further examined by means of AFM. In general, scan sizes ranging between 5 and 20 μm, were used with simultaneous acquisition of topography, height, error and phase images. A Park Systems XE-100 AFM was used in non-contact mode with a silicon cantilever. An adaptive scan rate between 0.15 Hz and 0.25 Hz was utilized for all samples. In Figure 8 topographical and error signal images of the textured surfaces described above are shown. To acquire a high quality AFM image of a surface with micrometer features, the deflection (or amplitude) signals (which represent the error signals) have to be minimized. If these signals are minimum, the error images obtained during scanning should look identical to the topographical features. 'Topography' images are generated by displaying the changes in the Z direction of the piezoelectric scanner required to restore the deflection of the cantilever to its predefined set point at each image point. Displaying the transient deviations of the cantilever away from the set point as the tip encounters features during scanning generates the 'error signal' image. It effectively represents a differential of the topography image, since it accentuates sharp turning points in the sample topography (high frequency information) at the expense of smooth slowly undulating areas (low frequency information). Indeed, both the topographical and the error signal images in Figure 8 match perfectly, indicating that there exist no additional phases or impurities on the laser textured surface as a result of the laser exposure. Moreover, from these images, it is seen that the surface topography is made up of collective pyramidal structures which probably were carved out of larger surface bumps during laser ablation. In Figure 9 it is presented a high magnification AFM topography signal of the patterned surface corresponding to Figure 8. In this image the

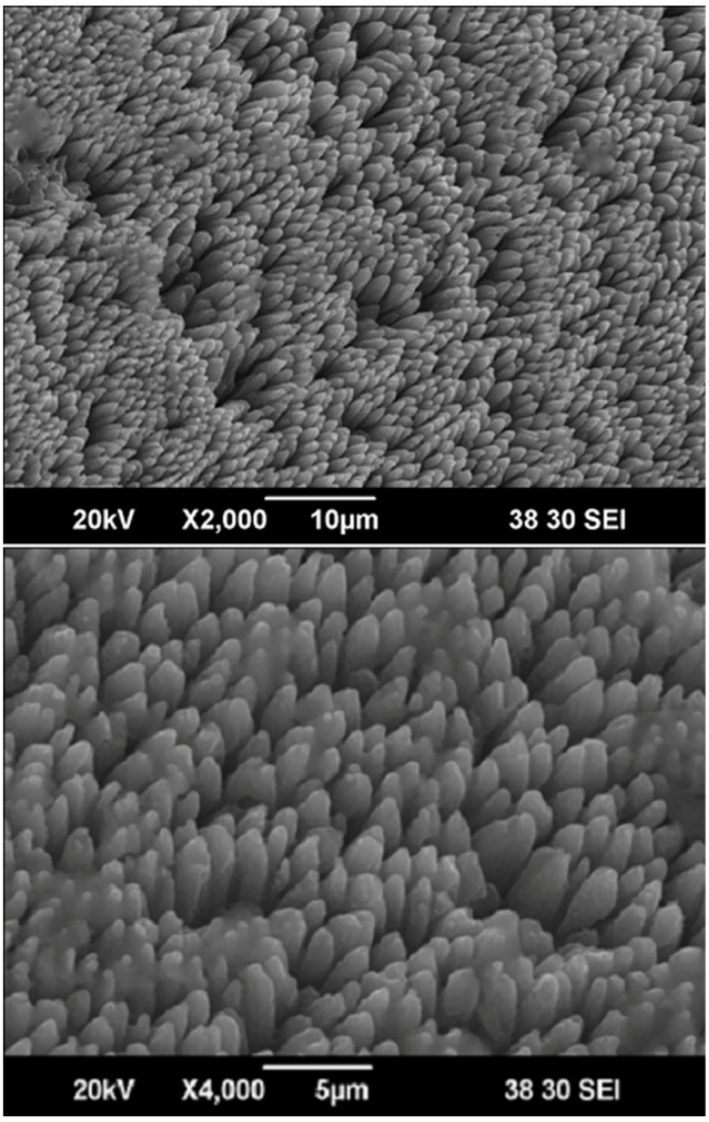

Figure 7. SEM images of low magnification (top) and high magnification (bottom) from a laser-ablated area on a silicon wafer. Closely packed pyramid-like roughness features of average size of 2 μm can be distinguished [5].

morphology of the pyramid-like roughness can be seen in detail. These textured surfaces were realized with a UV nanosecond laser working with a laser fluence of 1 J/cm^2.

From the abovementioned images it can be concluded that four pyramid-like roughness features are packed into a 25 μm^2 silicon surface. Also the base of the pyramids is made up of a layered structure, most probably originating from the laser induced melting-solidification cycles [34]. Roughness analysis indicates that the base of the pyramids is about 2 μm wide and the top is 0.5 μm wide. The size, depth and the distribution of the resultant protruding features, strongly depends on the laser parameters (beam energy and focus spot area). In this case, the samples were prepared by irradiating the wafers with a line focused beam of about 20 mm in length and 0.2 mm in width while rotating the wafer. The line focus is set radially; starting

http://dx.doi.org/10.5772/56173

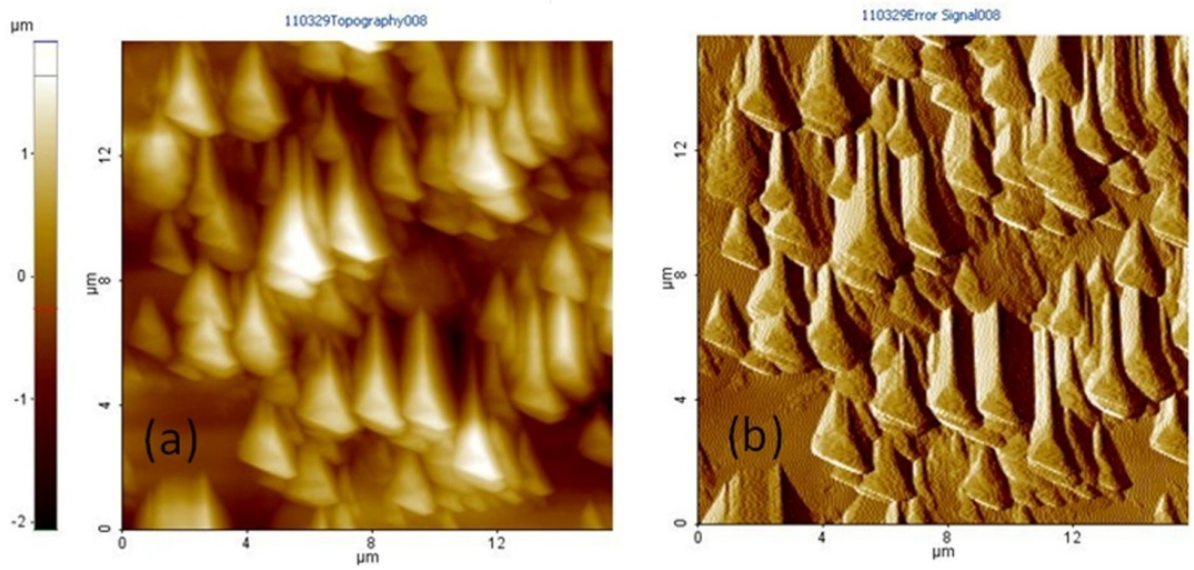

Figure 8. AFM topographical (a) and error signal images (b) corresponding to a laser-textured surface using the UV nanosecond laser at a fluence of 1 J/cm^2 [5].

slightly from the center of the wafer, thus the actual shot dose (i.e. number of laser shots per unit surface area) is changing along the radius.

For the wetting characterization of the surfaces we used the same systems as described in Chapter 2. For water droplet adhesion measurements we used the following method: a water droplet is placed on the surface examined and then, the surface is slowly tilted while a CCD camera captures the changes in the droplet's shape. In the last recorded image, before the droplet's base starts to move, the advancing θ_A and receding θ_B APCA are measured. The difference of the advancing and receding APCA is the CAH. The standard deviation in all the measurements is ±3°. The surfaces of the ablated silicon shown in the Figures 7, 8 and 9 are superhydrophilic. Finite APCAs could not be measured on these surfaces since the water droplets that are placed are completely spread on them after a few seconds from the deposition. For practical purposes an APCA of 0° is assigned.

When PTFE particles are adhered to the laser-formed asperities of the surface by the triboelectric deposition method, the surface morphology and the wetting characteristics of the original surface change drastically. Two main factors were found to influence the final wetting properties of the composite surface. These are the substrate micro-roughness and the amount of the PTFE sub-micrometer particles that are adhered on it. In Figure 10, two 3D AFM topographic images of an untreated laser textured surface and a triboelectrically deposited PTFE surface on top of the textured surface are presented. The composite hydrophobic surface in Figure 10b displayed an APCA of 135° with CAH of 25°.

The contact angle of a smooth PTFE surface is around 110°. In this case, due to the underlying roughness the APCA is exceeding this value. Detailed APCA and CAH measurements showed that laser-textured silicon surfaces having an average roughness of ~ 5 µm do not become superhydrophobic (APCA > 150°) when coated with triboelectrically charged PTFE particles.

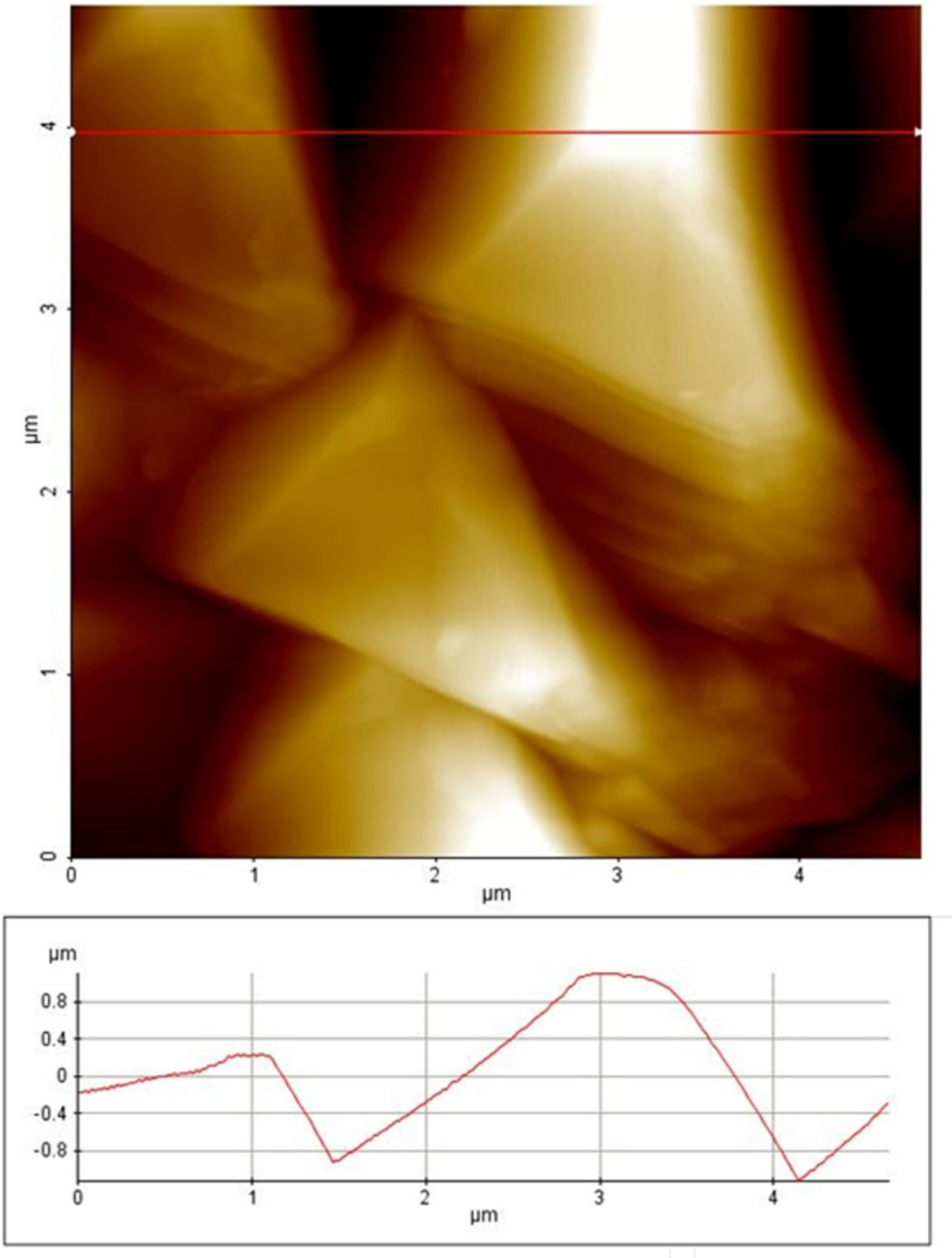

Figure 9. Top: AFM topography of a 5 µm × 5 µm surface area of the laser-microtextured silicon wafer surface. Bottom: Typical roughness profile of the micro-textured surface [5].

The composite hydrophobic surfaces obtained in this way showed relatively high CAH compared to a self-cleaning superhydrophobic surface (CAH < 10°). In average, the CAH obtained was 35°. In Figure 11, detailed APCA and CAH are presented for textured surfaces coated with PTFE. Four different textured surfaces were used as substrates, as a result of the four different laser fluencies that were used for their irradiation (0.5, 1.0, 1.5, and 2.0 J/cm^2).

http://dx.doi.org/10.5772/56173

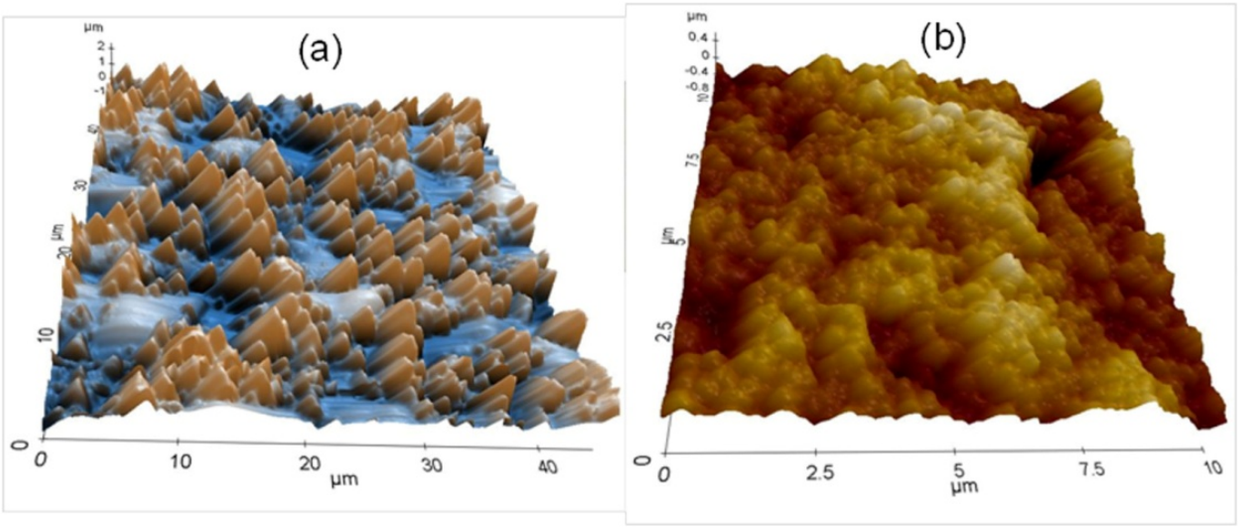

Figure 10. (a) A 3D AFM topography large area scan of textured silicon wafer surface before tribolelectric PTFE adhesion and (b) 3D topographical detail of the resultant surface roughness after the PTFE deposition [5].

Within the range of the laser fluencies that were studied, no major changes in the roughness of the silicon wafer were observed. However, the shape of the individual pyramid like microstructures could be modified without this having an effect on the final wetting properties of the PTFE coated surfaces. As seen in Figure 11, APCAs center around 130° and CAH around 35° for all the surfaces prepared. Although these surfaces cannot be considered superhydrophobic self-cleaning surfaces, water droplets exhibit quite low water adhesion on them and relatively high hydrophobicity. These wetting characteristics outperform certain hydrophobic polymers such as smooth PTFE or poly(dimethyl siloxane) (PDMS).

The four different laser fluencies that were used showed almost identical hydrophobicity. The main reason for this is attributed to the fact that the triboelectric coating creates 1.5 μm thick PTFE films. Therefore, the realization of a conformal superhydrophobic coating was not possible with the resultant silicon wafer surface roughness which was ranging from 2 to 5 μm. In order to circumvent this problem, SiC sandpapers were used of various grit sizes to analyze the effect of surface-microtexture on the degree of final hydrophobicity as a result of triboelectric PTFE deposition. Figure 12 shows that by tailoring the amount of PTFE adhered per unit area, surface hydrophobicity can be tuned from hydrophobic to self-cleaning superhydrophobic as a function of the surface micro-roughness. In general, for micro-rough surfaces up to 60 μm surface roughness, less than 1.5 mg/cm^2 PTFE attachment is enough to render them superhydrophobic. The rectangular region in Figure 12 indicates the roughness range which could be created by the UV laser micromachining of the silicon wafers. Figure 13 shows measured APCA and CAH as a function of the PTFE quantity deposited on a sandpaper of an average roughness of 16 μm. The best results (APCA > 155° and CAH < 20°) are obtained when the mass of PTFE deposited per surface area is approximately 0.5-0.7 mg/cm^2. A similar analysis on the laser-microtextured silicon wafer shows that much less amount of PTFE per unit area (0.05-0.15 mg/cm^2) is necessary to render the surface hydrophobic (Figure 14). In the case of the laser-textured silicon wafers, the amount of PTFE deposited is not affecting the

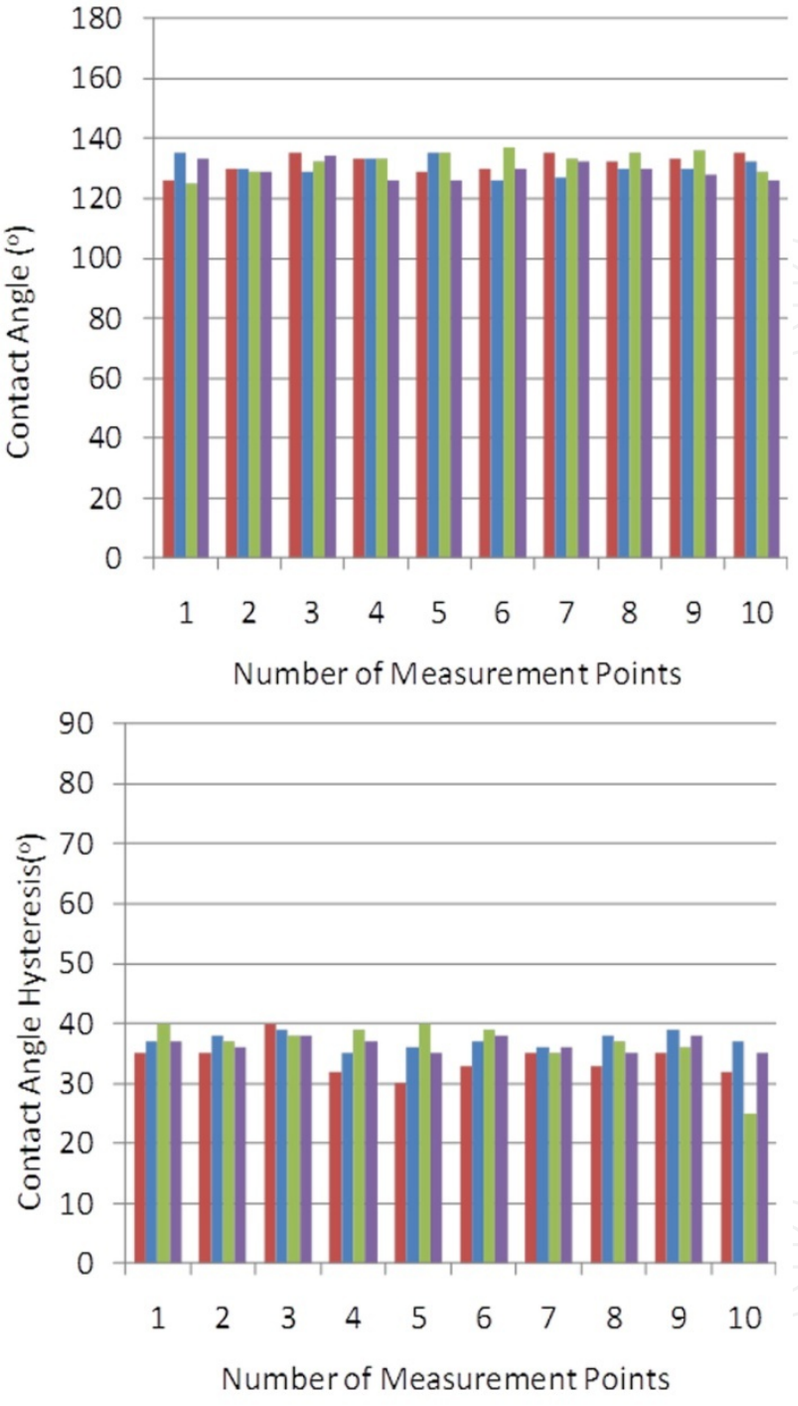

Figure 11. The results from 10 individual measurement points of the APCA and the CAH on PTFE coated laser-textured silicon wafers. The different colors in the graphs indicate the four different laser fluencies used ranging from 0.5 up to 2.0 J/cm^2. The measurements were performed randomly on different parts of the sample to investigate their homogeneity [5].

APCA and the CAH values in such a nice and controllable manner as in the case of the SiC sandpapers.

http://dx.doi.org/10.5772/56173

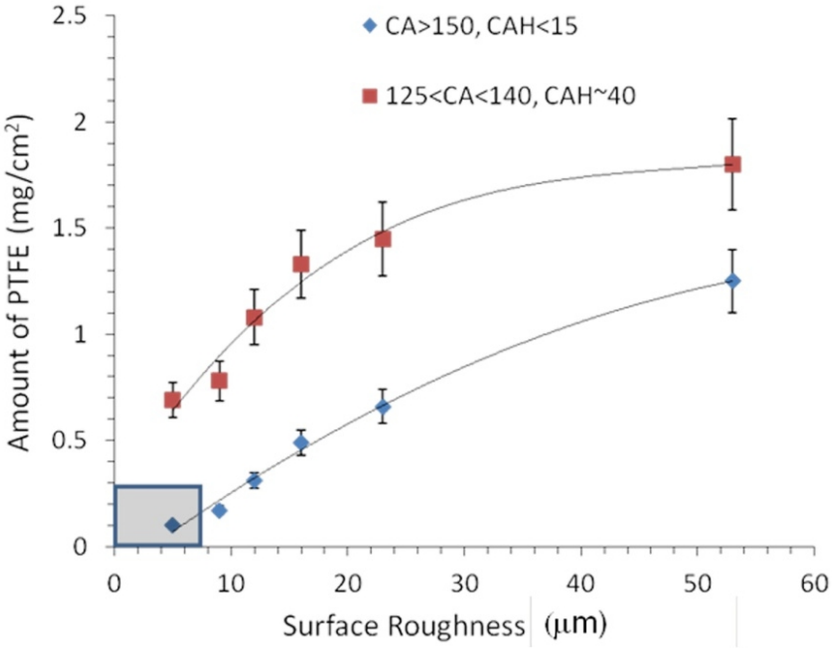

Figure 12. Effect of the amount of PTFE deposited as a function of the surface roughness on the degree of hydrophobicity and water adhesion. The grey box indicates the roughness regions obtained with the UV laser micromachining of the silicon wafers. The surface roughness out of this region is due to the use of SiC sandpapers with different grit sizes. The data set given (CA > 150°, CAH < 15°) indicates self-cleaning superhydrophobicity [5].

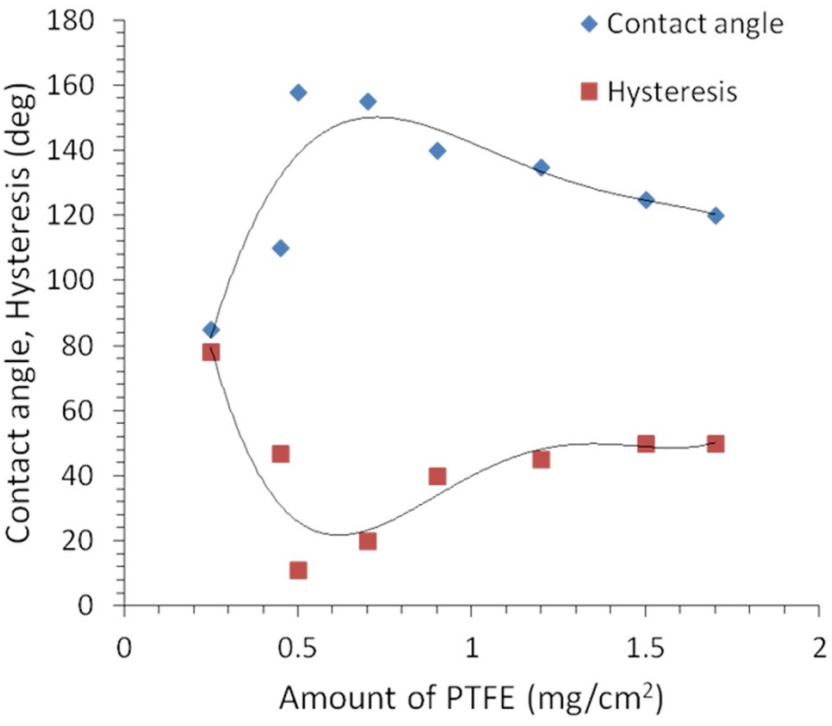

Figure 13. Effect of the amount of PTFE deposited on sandpaper with an average roughness of 16 μm, on the degree of the final hydrophobicity and water adhesion. PTFE measurements were accurate to 0.1 mg/cm² [5].

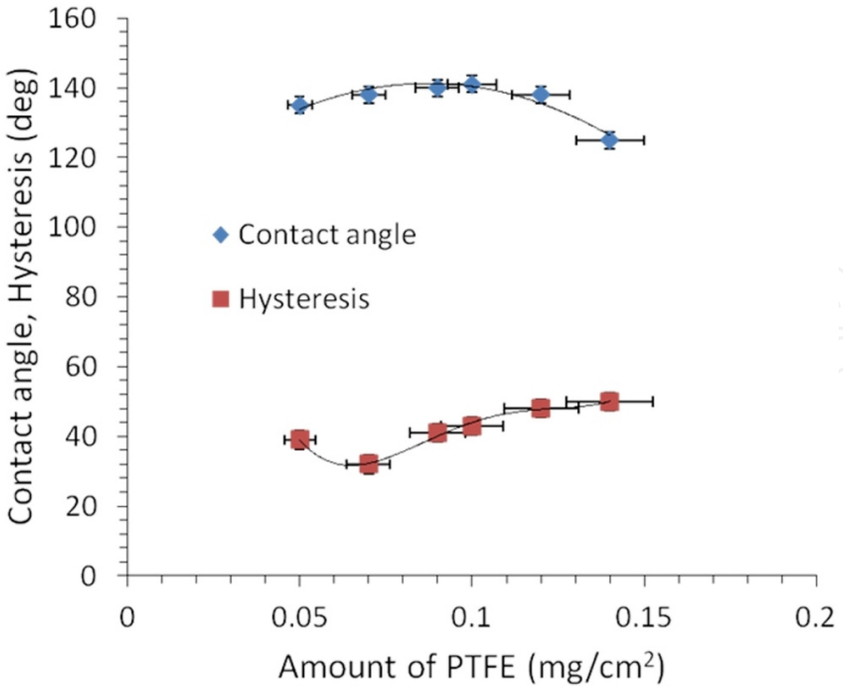

Figure 14. Effect of the amount of PTFE deposited on a laser-textured surface with average roughness of 2 μm, on the degree of the final hydrophobicity and water adhesion [5].

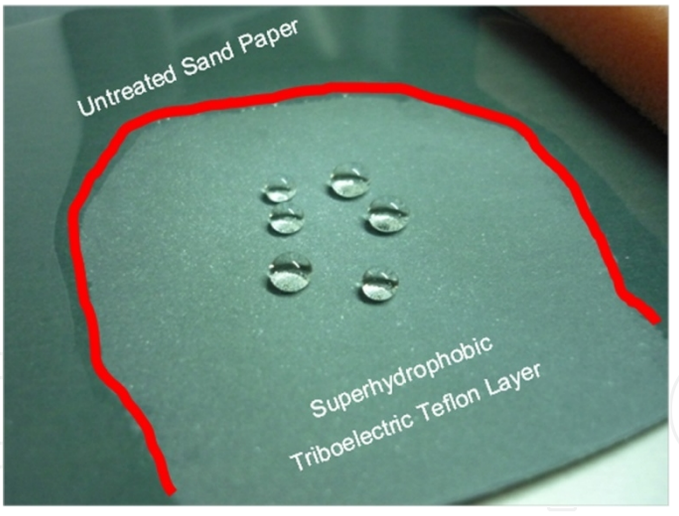

Figure 15. Photograph of a 600 grit SiC sandpaper with a treated with PTFE region and an untreated region. It is clear the difference in the wetting properties of the two surface areas [5].

Finally, in Figure 15, it is shown a photograph of a sandpaper (600 grit, average roughness: 26 μm). A part of which was coated with the triboelectric PTFE deposition and the other was left untreated. The red line in the photo shows the boarders between the treated and untreated region. As it can be observed, the untreated region is completely wet whereas in the treated region the droplets are in a superhydrophobic state.

http://dx.doi.org/10.5772/56173

4. Conclusions

In this work, we demonstrated two different lithography techniques, each one in combination with a different coating method. The purpose of these two fabrication processes is to obtain surfaces with large areas exhibiting special wetting characteristics with a simple, efficient, repeatable and economical strategy. The first process consists of the fabrication of SU-8 micropillar patterns on silicon by means of UV lithography. The patterns are subsequently coated by spraying particles which induce different roughness scales (submicrometer roughness with PTFE and nano-roughness with iron oxide). The substrates, starting from "sticky" hydrophobic (SU-8 uncoated patterned surfaces), by the application of the proper particles, can be converted to superhydrophobic surfaces with ultrahigh or ultralow water adhesion. The second process combines the laser micromachining of silicon wafers with the coating method of triboelectric deposition of charged PTFE submicrometer particles. This green solvent-free fabrication method results in surfaces with dual scale roughness (in micro- and nano-scale). These surfaces, upon the coating application are converted from superhydrophilic to hydrophobic (APCA = 130°) with low water adhesion (CAH ~ 35°). If instead of the silicon wafers are used SiC sandpapers with various grit sizes, then after the triboelectric deposition of PTFE the surfaces become superhydrophobic. The methods described here can find application in the development of microfluidic devices, smart surfaces, biotechnological materials and generally in all kinds of applications that special wetting properties and controllable roughness is required.

Acknowledgements

The authors would like to thank Dr Luigi Martiradonna, Dr George C. Anyfantis, Dr P. Davide Cozzoli and Professor Roberto Cingolani for their contribution in this work, as well as Mr Diego Mangiulo, Mr Gianmichele Epifani and Mr Paolo Cazzato for their technical assistance during the experimental process.

Author details

Athanasios Milionis[1], Ilker S. Bayer[1], Despina Fragouli[1], Fernando Brandi[1] and Athanassia Athanassiou[1*]

*Address all correspondence to: athanassia.athanassiou@iit.it

1 Nanophysics, Istituto Italiano di Tecnologia (IIT), Genoa, Italy

Smart Materials, Center for Biomolecular Nanotechnologies@UNILE, Arnesano (LE), Italy

References

[1] Xia, D, Johnson, L. M, & Lopez, G. P. Anisotropic wetting surfaces with one-dimensional and directional structures: fabrication approaches, wetting properties and potential applications. Advanced Materials (2012). , 24(10), 1287-1302.

[2] Liu, M, & Jiang, L. Switchable adhesion on liquid/solid interfaces. Advanced Functional Materials (2010). , 20(21), 3753-3764.

[3] Lee, J. B, Gwon, H. R, Lee, S. H, & Cho, M. Wetting transition characteristics on microstructured hydrophobic surfaces. Materials transactions (2010). , 51(9), 1709-1711.

[4] Milionis, A, Martiradonna, L, Anyfantis, G. C, Cozzoli, P. D, Bayer, I. S, Fragouli, D, & Athanassiou, A. Control of the water adhesion on hydrophobic micropillars by spray coating technique. Colloid and Polymer Science (2013). , 291(2), 401-407.

[5] Bayer, I. S, Brandi, F, Cingolani, R, & Athanassiou, A. Modification of wetting properties of laser-textured surfaces by triboelectrically charged Teflon particles. Colloid and Polymer Science (2013). , 291(2), 367-373.

[6] Tsougeni, K, Papageorgiou, D, Tserepi, A, & Gogolides, E. Smart" polymeric microfluidics fabricated by plasma processing: controlled wetting, capillary filling and hydrophobic valving. Lab on a Chip (2010). , 10(4), 462-469.

[7] Villafiorita-monteleone, F, Mele, E, Caputo, G, Spano, F, Girardo, S, Cozzoli, P. D, Pisignano, D, Cingolani, R, Fragouli, D, & Athanassiou, A. Optically controlled liquid flow in initially prohibited elastomeric nanocomposite micro-paths. RSC Advances (2012). , 2(25), 9543-9550.

[8] Stratakis, E, Ranella, A, & Fotakis, C. Biomimetic micro/nanostructured functional surfaces for microfluidic and tissue engineering applications. Biomicrofluidics (2011).

[9] Kannarpady, G. K, Lefrileux, Y, Laurent, J, Woo, J, Khedir, K. R, Ishihara, H, Trigwell, S, Ryerson, C, & Biris, A. S. Nanotech (2010). conference proceedings, June Anaheim Convention Center, Anaheim, CA, USA., 21-24.

[10] Huang, X. J, Kim, D. K, Im, M, Lee, J. H, Yoon, J. B, & Choi, Y. K. Lock-and-key" geometry effect of patterned surfaces: wettability and switching of adhesive force. Small (2009). , 5(1), 90-94.

[11] Furstner, R, Barthlott, W, Neinhuis, C, & Walzel, P. Wetting and self-cleaning properties of artificial superhydrophobic surfaces. Langmuir (2005). , 21(3), 956-961.

[12] Feng, J, Tuominen, M. T, & Rothstein, J. P. Hierarchical superhydrophobic surfaces fabricated by dual-scale electron-beam lithography with well-ordered secondary nanostructures. Advanced Functional Materials (2011). , 21(19), 3715-3722.

[13] Shirtcliffe, N. J, Aqil, S, Evans, C, Mchale, G, Newton, M. I, Perry, C. C, & Roach, P. The use of high aspect ratio photoresist (SU-8) for super-hydrophobic pattern prototyping. Journal of Micromechanics and Microengineering (2004). , 14(10), 1384-1389.

[14] Marquez-velasco, J, Vlachopoulou, M. E, Tserepi, A. D, & Gogolides, E. Stable superhydrophobic surfaces induced by dual-scale topography on SU-8. Microelectronic Engineering (2010).

[15] Wagterveld, R. M, Berendsen, C. W. J, Bouaidat, S, & Jonsmann, J. Ultralow hysteresis superhydrophobic surfaces by excimer laser modification of SU-8. Langmuir (2006). , 22(26), 10904-10908.

[16] He, Y, Jiang, C, Yin, H, Chen, J, & Yuan, W. Superhydrophobic silicon surfaces with micro-nano hierarchical structures via deep reactive ion etching and galvanic etching. Journal of Colloid and Interface Science (2011). , 364(1), 219-229.

[17] Athanassiou, A, Fragouli, D, Villafiorita-monteleone, F, Milionis, A, Spano, F, Bayer, I. S, & Cingolani, R. Laser-based lithography for polymeric nanocomposite structures. In: Cui B. (ed.) Recent advances in nanofabrication techniques and applications. Rijeka: Intech; (2012). , 289-314.

[18] Andrzejewska, E. Photopolymerization kinetics of multifunctional monomers. Progress in Polymer Science (2001). , 26(4), 605-665.

[19] Hong, L, & Pan, T. Photopatternable superhydrophobic nanocomposites for microfabrication. Journal of Microelectromechanical Systems (2010). , 19(2), 246-253.

[20] Caputo, G, Cortese, B, Nobile, C, Salerno, M, Cingolani, R, Gigli, G, Cozzoli, P. D, & Athanassiou, A. Reversibly light-switchable wettability of hybrid organic/inorganic surfaces with dual micro-/nanoscale roughness. Advanced Functional Materials (2009). , 19(8), 1149-1157.

[21] Debuisson, D, Senez, V, & Arscott, S. Tunable contact angle hysteresis on micropatterned surfaces. Applied Physics Letters (2011).

[22] Calcagnile, P, Fragouli, D, Bayer, I. S, Anyfantis, G. C, Martiradonna, L, Cozzoli, P. D, Cingolani, R, & Athanassiou, A. Magnetically driven floating foams for the removal of oil contaminants from water. ACS Nano (2012). , 6(6), 5413-5419.

[23] Balu, B, Breedveld, V, & Hess, D. W. Fabrication of “roll-off” and “sticky” superhydrophobic cellulose surfaces via plasma processing. Langmuir (2008). , 24(9), 4785-4790.

[24] Quere, D, Lafuma, A, & Bico, J. Slippy and sticky microtextured solids. Nanotechnology (2003). , 14(10), 1109-1112.

[25] Feng, L, Zhang, Y, Xi, J, Zhu, Y, Wang, N, Xia, F, & Jiang, L. Petal effect: a superhydrophobic state with high adhesive force. Langmuir (2008). , 24(8), 4114-4119.

[26] Bormashenko, E, Stein, T, Pogreb, R, & Aurbach, D. Petal effect" on surfaces based on lycopodium: high-stick surfaces demonstrating high apparent contact angles. Journal of Physical Chemistry C (2009). , 113(14), 5568-5572.

[27] Cassie, A. B. D, & Baxter, S. Wettability of porous surfaces. Transactions of the Faraday Society (1944). , 40(0), 546-551.

[28] Zhu, L, Feng, Y, Ye, X, & Zhou, Z. Tuning wettability and getting superhydrophobic surface by controlling surface roughness with well-designed microstructures. Sensors and Actuators A (2006). SI) , 595-600.

[29] He, Y, Jiang, C, Yin, H, Chen, J, & Yuan, W. Superhydrophobic silicon surfaces with micro-nano hierarchical structures via deep reactive ion etching and galvanic etching. Journal of Colloid and Interface Science (2011). , 364(1), 219-229.

[30] Feng, J, Tuominen, M. T, & Rothstein, J. P. Hierarchical superhydrophobic surfaces fabricated by dual-scale electron-beam-lithography with well-ordered secondary nanostructures. Advanced Functional Materials (2011). , 21(19), 3715-3722.

[31] Teisala, H, Tuominen, M, Aromaa, M, Stepien, M, Makela, J. M, Saarinen, J. J, Toivakka, M, & Kuusipalo, J. Nanostructures increase water droplet adhesion on hierarchically rough superhydrophobic surfaces. Langmuir (2012). , 28(6), 3138-3145.

[32] Wang, X, Mak, G. Y, & Choi, H. W. Laser micromachining and micro-patterning with a nanosecond UV laser. In: Kahrizi M. (ed.) Micromachining techniques for fabrication of micro and nano structures. Rijeka: Intech; (2012). , 85-108.

[33] Fadeeva, E, Truong, V. K, Stiesch, M, Chichkov, B. N, Crawford, R. J, Wang, J, & Ivanova, E. P. Bacterial retention on superhydrophobic titanium surfaces fabricated by femtosecond laser ablation. Langmuir. (2011). , 27(6), 3012-3019.

[34] Leitz, K. H, Redlingshöfer, B, Reg, Y, Otto, A, & Schmidt, M. Metal ablation with short and ultrashort laser pulses. Physics Procedia (2011). , 12-230.

[35] Kalyva, M, Bertoni, G, Milionis, A, Cingolani, R, & Athanassiou, A. Tuning of the characteristics of Au nanoparticles produced by solid target laser ablation into water by changing the irradiation parameters. Microscopy research and technique (2010). , 73(10), 937-943.

[36] Bayer, I. S, Caramia, V, Biswas, A, Cingolani, R, & Athanassiou, A. Metal-like conductivity exhibited by triboelectrically deposited polyaniline (emeraldine base) particles on microtextured SiC surfaces. Applied Physics Letters (2012). , 100-201604.

[37] Liu, C, & Bard, A. J. Electrostatic electrochemistry at insulators. Nature Materials (2008). , 7-505.